

Polymer Retention “Tailing” Phenomenon Associated with the Milne Point Polymer Flood

R. S. Seright^{1*} and Dongmei Wang²

¹New Mexico Tech

²University of North Dakota

Summary

Associated with the Milne Point polymer flood (on Alaska’s North Slope), this paper explores the unusual shape of hydrolyzed polyacrylamides (HPAM) breakout/propagation during dynamic polymer retention measurements in Milne Point core material. In contrast to conventional expectations, polymer retention does not delay the initial polymer arrival at the end of a Milne Point core. However, after effluent polymer concentrations rapidly rise to at least 50% of the injected value, the concentration gradually “tails” up over many pore volumes (PVs) before it finally achieves the injected value. To understand the origin and significance of this behavior, a wide range of core experiments were performed, including substantial variations in polymer concentration and molecular weight, core length, preservation state, sand grain size, and mineral composition. Illite was identified as primarily responsible for the tailing phenomenon. This phenomenon has important consequences that must be considered when projecting the performance of the field project. This work suggests that mineralogy analysis (especially for illite and kaolinite) may reveal whether tailing should be accounted for during simulations of polymer propagation/retention in a given field application.

Introduction

The Milne Point polymer flood is a very successful Department-of-Energy-sponsored pilot project, directed at a recovery of ~300 cp oil on the Alaskan North Slope. This project has seen produced water cuts drop from ~70% during waterflooding before the project to less than 10% during polymer injection. Many aspects of this project are documented in Chang et al. (2020); Dandekar et al. (2019, 2020, 2021); Dhaliwal et al. (2021); Ning et al. (2019); Wang et al. (2020, 2022) and Zhao et al. (2021). This paper focuses on how polymer retention might impact the Milne Point polymer flood.

In any polymer flood or chemical flood where the polymer is used for mobility control, the polymer must propagate deep into the porous rock of the reservoir to be effective. Polymer retention (e.g., adsorption and mechanical entrapment) can retard the movement of polymer solutions through the reservoir and thus have an important impact on the efficiency of oil displacement and the economics of a project (Manichand and Seright 2014; Wang et al. 2020). Projections of the impact of polymer retention on a given field project are commonly incorporated into numerical simulations and/or fractional flow calculations (Green and Willhite 2018). Chemical flooding simulators traditionally assume that polymer retention follows the Langmuir isotherm, while fractional-flow calculations usually assume concentration-independent retention. Both models predict a delay in propagation of the polymer front (in proportion to the given retention value), followed by a rapid rise in produced polymer concentration to the injected level. For illustration, the blue curve in **Fig. 1** shows polymer propagation predictions using the Langmuir isotherm (in a simulator), while the black-dashed curve shows predictions from an assumption of concentration-independent retention using fractional flow calculations (all assuming 240 µg/g total polymer retention). In contrast, our laboratory retention studies (Wang et al. 2020) for the Milne Point polymer flood (North Slope of Alaska) consistently showed virtually no delay in polymer propagation, a rapid rise in produced polymer to 70–90% of the injected concentration, followed by produced concentration gradually approaching the injected value over many PV. This tailing behavior yields an overall retention of up to 600 µg/g, even though most polymer is not delayed. From a practical viewpoint, this behavior means that retention causes no significant delay in propagation of the polymer bank (and therefore the oil bank), but the effective viscosity and displacement efficiency are less than originally planned. This paper explores why this polymer “tailing” phenomenon occurs.

Detailed aspects of polymer retention were covered during previous reviews (Manichand and Seright 2014; Zhang and Seright 2014; Seright 2017; Wever et al. 2018; Green and Willhite 2018; Guetni et al. 2019; Ferreira and Moreno 2020; Wang et al. 2020; Sugar et al. 2021). However, only Wang et al. (2020) mentioned the tailing phenomenon. Perhaps this phenomenon was not reported previously for fear that the effect might have been an experimental artifact associated with the polymer retention method used. However, in Wang et al. (2020) (and again in this work), three different polymer retention methods were used simultaneously to demonstrate that the tailing phenomenon was a real effect. In addition to the tailing phenomenon, Wang et al. noted that inaccessible pore volume (IAPV) was negligible in Milne Point cores. They also found no evidence of chromatographic separation of HPAM molecular weights during dynamic retention experiments—the intrinsic viscosity of the first polymer produced from a core was (within experimental error) the same as that produced many PV later.

In this paper, multiple types of laboratory measurements were used to assess HPAM polymer retention. Core floods were used to dynamically determine polymer retention in different Milne Point Schrader Bluff sands, with extensive permeability, grain size distribution, X-ray diffraction, and X-ray fluorescence characterizations. During all experiments, the effluent was analyzed for brine-tracer concentration, viscosity, total organic carbon, and total nitrogen. The latter three items allowed three independent measures of polymer concentration and polymer retention. The first experiments described in this paper were performed with Milne Point core material, oil, brine, and conditions. We investigated the effects of core preservation state [extending those studies described in Wang et al. (2020)]. Additional studies were performed to quantify how the tailing phenomenon varied with injection rate, polymer concentration and

*Corresponding author; email: randy.seright@nmt.edu

Copyright © 2022 Society of Petroleum Engineers

Original manuscript received for review 27 December 2021. Revised manuscript received for review 4 February 2022. Paper (SPE-209354-PA) peer approved 24 February 2022.

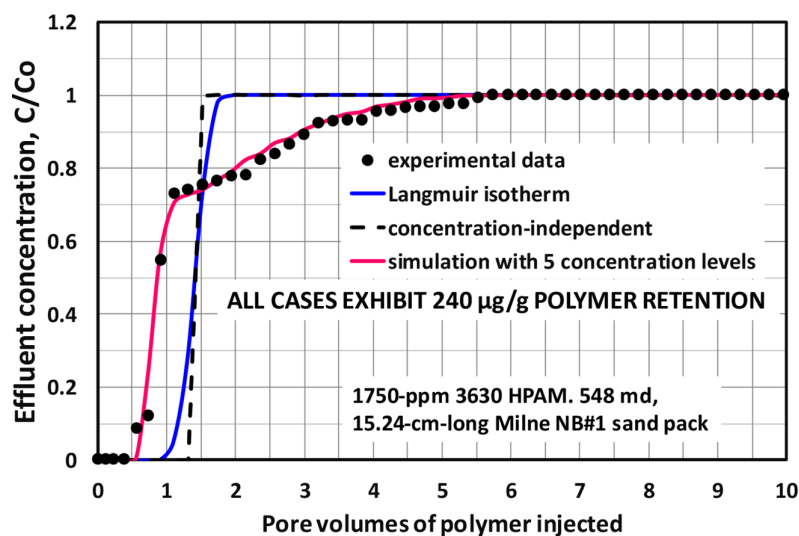


Fig. 1—Tailing phenomenon during a polymer retention study vs. model predictions.

molecular weight (Mw), and sand grain particle size in Milne Point sands. Subsequently, mechanistic experiments are presented using packs of glass beads with controlled levels of various minerals, including illite, kaolinite, montmorillonite, chlorite, calcium carbonate, dolomite, siderite, pyrite, and calcium sulfate. Next, extensive experiments are analyzed that focus on bead packs containing illite—the most prevalent clay in Milne Point core material. These experiments examine a wide range of polymer concentrations and Mw values, flow rates, core lengths, and particle sizes. In the end, a model is proposed to account for the tailing phenomenon.

Materials and Methods

The Brine, Polymers, and Polymer Solutions. The synthetic brine in this work was called Milne Point injection water, which contained 2,435-ppm TDS (not including water of hydration)—consisting of 2,173-ppm NaCl, 8-ppm KCl, 357-ppm $\text{CaCl}_2 \cdot 2\text{H}_2\text{O}$, and 73-ppm $\text{MgCl}_2 \cdot 6\text{H}_2\text{O}$. The calcium and magnesium salts were added as hydrates. This brine was passed through 0.45- μm Millipore filters before further use.

For most of this work, several powder-form partially HPAM were used: SNF Flopaam 3630STM (Lot GJ1201, received from the Milne Point field application 26 September 2018), SNF Flopaam 3430STM, SNF Flopaam 3130STM, and Flodrill TS705TM. The degree of hydrolysis was 30% for these polymers. In one experiment, Ciba Alcoflood 254 STM was used, which had a 10% degree of hydrolysis. The third column of **Table 1** lists manufacture-stated Mw ranges (based on intrinsic viscosity). We made our own measurements of intrinsic viscosity and Mw in the Milne Point injection water, using the methods of Jouenne and Levache (2020). These Mw values are listed in the fourth column, while the fifth column lists C^* values—the critical polymer overlap concentration. Below this concentration, polymer molecules generally float free and unentangled in solution. Above this concentration, the polymer molecules are entangled with others.

Polymer	Anionicity (%)	Manufacturer-Stated Mw (million g/mol)	Measured Mw (million g/mol)	C^* (ppm)
Flopaam 3630S	30	17–19	18*	200
Flopaam 3430S	30	10–12	11	300
Flopaam 3130S	30	3–5	2.7	850
Flodrill TS705	30	-	0.3	4,500
Alcoflood 254S	10	0.25–0.5	0.1	10,000

*This case was used as a starting basis for the calculations and comparison.

Table 1—Mw and C^* parameters for HPAM polymers.

Polymer solutions were prepared by sprinkling polymer powder (over the course of 4 minutes) onto the brine vortex created by an overhead stirrer (IKA RW-200) at 300 rev/min with a four-blade propeller. After initial mixing for several hours at a high rate, the stir rate was reduced to ~100 rev/min for at least 1 day. Polymer solutions were confirmed to be homogeneous by the absence of any lumps within a thin layer as the fluid flowed over a beaker lip when poured from one beaker to another. As in the field application, our target polymer solution viscosity was 45 cp (at 7.3 second^{-1} 25°C). For consistency in many studies, we fixed concentrations at 1,750-ppm Flopaam 3630S and 2,000-ppm Flopaam 3430S.

The Sands. The Schrader Bluff sands of the Milne Point polymer flood were the NB sand and the OA sand. (These labels are simply the names assigned to specific sand formations by the original field developer.) The current polymer pilot is flooding NB sands, but OA sands are of high interest for expansion of the polymer flood. Our experiments used NB sands (provided by Hilcorp) from two different wells (located 3,000 ft apart and at slightly different depths). We labeled NB sands from 3,908 ft of the Pesado well as “NB1”; and NB sands from 3,757 ft of the Liviano well as “NB3.” The OA sand used in this work was from 4,067 ft of the Pesado well. The sands are

fairly similar in elemental composition, except the OA sand contains five to seven times as much calcium, 30% more iron, 30–100% more magnesium, and 70–90% less sulfur than the NB sands. The NB3 sand had four to five times as much sulfur as the NB1 sand. The clay contents of the various sands were similar, with the NB3 sand containing slightly less than the others. The OA sand contained noticeably more dolomite and feldspar (albite and orthoclase) than the NB sands. Grain-size distributions were obtained for the sands and materials used to make synthetic sandpacks. These distributions were obtained using a laser-diffraction method (Malvern Mastersizer 3000™ with Hydro EV™ dispersing unit), which provides volume-based measurements.

Sandpack Preparation. Our packing procedures are described in Wang et al. (2020). Typically for the current work, we used biaxial Temco Hassler core holders. These were 2.54 cm in diameter and usually either 15.24 or 30.48 cm in length. To fine-tune the desired pack permeability, the confining pressure (i.e., overburden pressure) was varied (between 100 and 1,750 psi). However, 500 psi confining pressure was most commonly used, unless stated otherwise. GE Druck DPI 104™ pressure transducers were used—either 1,000 psi transducers with 0.1 psi readout or 300 psi transducers with 0.01 psi readout. Four ISCO (Model 500D or 1000D™) pumps were used during a typical experiment—one each for brine, polymer solution, oil, and confining pressure.

The condition of the sand varied (see **Table 2**). In some cases, the sand was used as received (“native state”), where some unquantified level of residual water and oil was present. Other times, the sand was washed/extracted with toluene and methanol and dried before use. In some cases, the sands were saturated only with brine before use. In other cases, the sandpacks were “restored”—that is, flooded with fresh Milne Point oil (viscosity ~111 cp at 25°C) to connate water saturation, followed by flooding with at least 150 PV of brine to drive the sandpack to residual oil saturation. Preserved cores were also used. (Preserved cores were carefully collected by the field operator during drilling/coring so that the wettability of the cores was maintained at or close to that within the reservoir. Furthermore, the cores were sealed and stored in a controlled environment to maintain their condition until use.) Note that all cores listed in **Table 2** contained some level of residual oil. Generally, the level of residual oil was not quantified—especially because that was not practical for native-state cores. Consistent with our experience with other oils, Chang et al. (2020) found no evidence that HPAM partitions from the water phase into Milne Point oil.

Figure/Curve	Sand	Sand Condition	k_w (md)	k_w at S_{or} (md)	ϕ^*	Length (cm)	Polymer Mw (g/mol)	Polymer (ppm)	Darcy Velocity (ft/d)
1	NB1	Restored	548	50	0.25*	15.24	18 million	1,750	3.7
2	OA	Native	-	232	0.19	15.24	11 million	2,000	3.7
3/Black	NB1	Native	-	287	0.21	15.24	18 million	1,750	3.7
3/Green	NB1	Native	-	203	0.20	15.24	18 million	1,750	1.86
3/Red	NB1	Native	-	216	0.22	15.24	18 million	1,750	0.31
5/Black	NB1	Native	-	47	0.18	15.24	18 million	1,750	1.86
5/Red	NB1	Native	-	676	0.24	15.24	18 million	1,750	1.86
6/Black	OA	Native	-	100	0.19	15.24	18 million	600	3.7
6/Green	OA	Native	-	113	0.21	15.24	18 million	1,200	3.7
6/Red	OA	Native	-	544	0.22	15.24	18 million	1,750	3.7
7/Black	OA	Native	-	232	0.19	15.24	11 million	2,000	3.7
7/Red	OA	Native	-	544	0.22	15.24	18 million	1,750	3.7
8	NB1	Preserved	-	200	0.21	6.7	18 million	1,750	0.93

Many additional cores and experiments are described in Wang et al. (2020).

*The first porosity listing gives the absolute porosity. The remaining values indicate the effective aqueous phase porosity at the resident oil saturation. This value was based on the 50% concentration value during breakout of the KI water tracer.

Table 2—Properties of Milne cores used in retention experiments.

For comparison, some experiments referenced in Wang et al. (2020) (using the same Milne Point core material) contained no oil. The mechanistic bead-pack studies in the last part of this paper (where illite and other materials were added) contained no oil.

Also, in **Table 2**, most of the “porosity” values (excepting the first listing) were based on the 50% concentration value during breakout of the iodide water tracer. Note that most of these values ranged from 0.18 to 0.22. However, because some unknown residual oil saturation was present, the actual porosity values were probably closer to the 0.25 value associated with the first listing. This point is of consequence in **Fig. 1**, because the experimental data and the red curve there break out notably before 1 PV. This earlier than expected breakout is because a residual oil saturation was present (that occupied some pore space). For all subsequent retention figures in this paper, the PV and “porosity” values were based on the 50% breakout of the aqueous tracer.

Flood Sequence and Polymer and Tracer Detection. After pack saturation, characterization, and stabilization of brine injection at a low rate (typically, 1.86 or 3.7 ft/d darcy velocity), 5–13 PV of the polymer solution was injected at a fixed rate, while monitoring pressure drops across the pack or pack sections.

Effluent from packs was analyzed by several methods. Routinely, we monitored a water tracer (20-ppm potassium iodide) using a Genesis 2™ spectrophotometer at a wavelength of 230 nm. Effluent polymer concentration was monitored by three methods: total organic carbon, total nitrogen, and viscosity. For total organic carbon, a Shimadzu TOC-L™ was used. We recognize that this measurement might be influenced by the presence of any oil. Total nitrogen was measured using chemiluminescence with a Shimadzu TNM-L™ unit. Viscosity was measured at 7.3 s⁻¹ (25°C) using proRheo LS-300™ and/or Vilastic VE™ rheometers. The previous measurements were made at 3–4 cm³ increments for each effluent sample.

Fig. 2 illustrates the results during 10 PV of polymer injection (2,000-ppm Flopaam 3430S) for a 15.24-cm-long pack with 232-md native-state OA sand with 500-psi confining pressure. In **Fig. 2**, all values are reported relative to the injected values. The dashed blue curve shows the tracer (KI) breakout. The black and green curves show breakout of the polymer, as judged by carbon content and nitrogen content, respectively. The solid red curve plots effluent produced polymer concentrations that were based on viscosities (using a relation between viscosity and concentration that was reported in Wang et al. 2020).

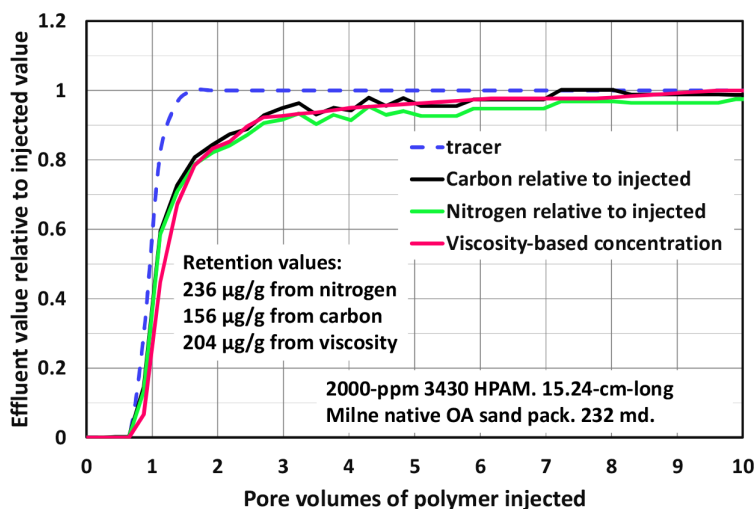


Fig. 2—Effluent composition during polymer injection (232-md native OA sand).

The difference in area between the tracer (dashed blue) curve and a given polymer curve in **Fig. 2** can be used to calculate polymer retention (if one assumes that IAPV is zero). Specifically, Eq. 1 (from Manichand and Sright 2014) provides a means for the calculations:

$$R_{pret} = \{[\Sigma[(C_p/C_{po} * \Delta PV) - (C_t/C_{to} * \Delta PV)]] + IAPV\} * C_{po} * PV/M_{rock}, \quad (1)$$

where R_{pret} is the polymer retention, C_p is the effluent polymer concentration, C_{po} is the injected polymer concentration, C_t is the effluent tracer concentration, C_{to} is the injected tracer concentration, PV is the volume in one PV, ΔPV is the pore-volume increment, and M_{rock} is the rock mass in the sandpack.

In **Fig. 2**, polymer retention values were 236 $\mu\text{g/g}$ based on effluent nitrogen, 156 $\mu\text{g/g}$ based on effluent carbon, and 204 $\mu\text{g/g}$ using viscosity-based concentration. The nitrogen-based calculation provides the most reliable answer because the carbon-based method could be influenced by any carbon contamination (e.g., residual oil) and polymer degradation could affect the viscosity-based method. To elaborate, if the produced carbon concentrations are higher than the nitrogen concentrations (because of the presence of oil), that makes the area between the tracer and carbon effluent curves smaller than that between the tracer and the nitrogen effluent curves—which in turn, makes polymer retention appear smaller for carbon detection than for nitrogen detection. Consequently, all subsequent retention values reported in this paper are based on nitrogen detection.

Uncertainties in Measurements. The jumps and fluctuations observed in **Fig. 2** give an indication of the uncertainties associated with the concentration measurements—typically appearing to be on the order of 5%. The device used to measure carbon and nitrogen content advertises that the error bars around a given measurement should be less than 1 or 2% (in agreement with our experience with this instrument). However, there can be unquantified uncertainties associated with the sample preparation process that increases the variation to the levels seen in **Fig. 2**. In comparing results from the Milne Point cores (**Figs. 1 through 8**), note that some variability is also added because of the natural core-to-core variations in mineral content and other characters. This aspect of the variation should be improved for the mechanistic bead-pack studies (**Figs. 9 through 19**) because the pack compositions were controlled.

Results in Milne Point Core Material

Effect of Fluid Velocity. It seemed conceivable that the tailing phenomenon is related to diffusion—so that the magnitude of the tail might be sensitive to the velocity at which the experiment was performed. To test this idea, separate retention experiments were performed at different rates, ranging from 0.31 to 3.7 ft/d (darcy velocity). These experiments used 1,750-ppm Flopaam 3630 S in 15.24-cm-long sandpacks of native NB1 sand that had permeability (to brine) ranging from 203 to 287 md. **Fig. 3** demonstrates that the rate did not significantly affect the shape of the polymer breakout curves. For the three cases, the effluent concentration rapidly rose to ~70% of the injected value (at 1.5 PV) and then tailed up to ~90% of the injected value after 10 PV. Overall retention values calculated at 10 PV ranged from 339 to 482 $\mu\text{g/g}$ —with most of the retention associated with the tail. Of the total retention values listed, 209–305 $\mu\text{g/g}$ was associated with the tailing phenomenon (i.e., materializing after 2 PV of polymer injection). Considering the variations seen in **Fig. 3**, we do not consider these values to be significantly different. Thus, the tailing phenomenon did not appear to be sensitive to fluid velocity. This point will be explored further using a wider range of rates with mechanistic bead packs (later in the paper).

Effect of Particle Size. A second thought was that perhaps the tailing phenomenon might depend on the particle size or size distribution of the sand. To test this concept, a portion of NB1 sand was sieved to produce two sand fractions: one fraction that was between 20 and 35 mesh (841–500 μm) and the other fraction that passed through a 35-mesh screen (<500 μm). **Fig. 4** shows the particle-size distributions of the two fractions, as measured using a Malvern Mastersizer™ 3000 particle size analyzer. The median particle sizes [Dv(50)] for the

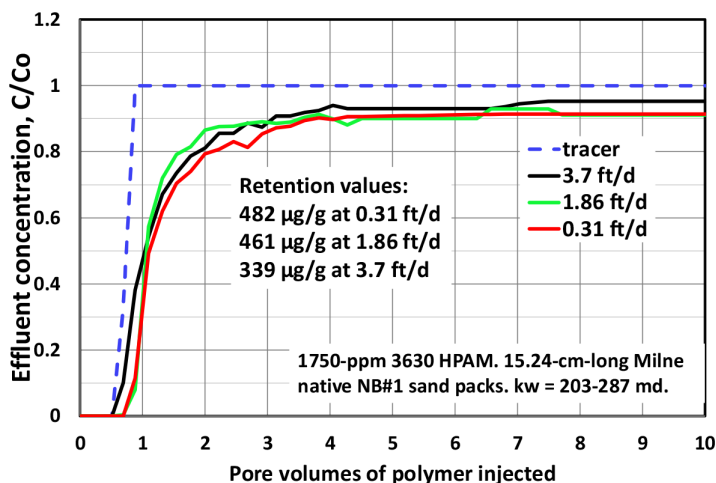


Fig. 3—Effect of rate on tailing phenomenon in native NB1 sandpacks.

two sand fractions were 692 and 231 μm , respectively, while the main peaks occurred at 666 and 211 μm , respectively. Fig. 5 compares results from two retention experiments using these two sand fractions, conducted under the same conditions. Retention values (determined at 10 PV polymer throughput) ranged from 337 to 461 $\mu\text{g/g}$, and the two effluent curves were quite similar. Thus, the tailing phenomenon did not appear to be sensitive to sand particle size (at least, under this range of conditions). Because this result is counterintuitive, we will further explore this point during mechanistic studies later in the paper.

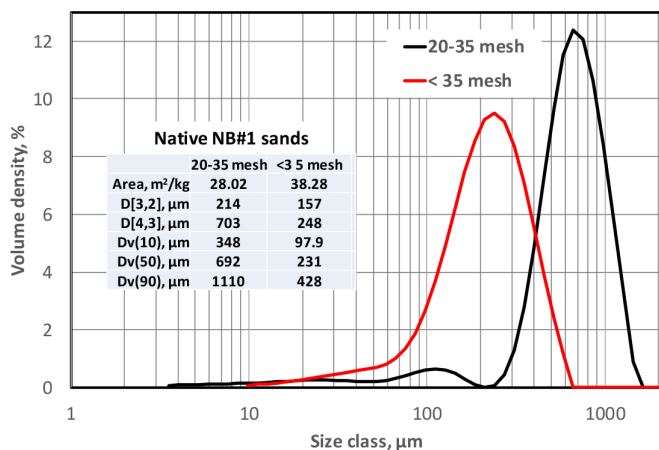


Fig. 4—Particle-size distributions for sieved NB1 sands.

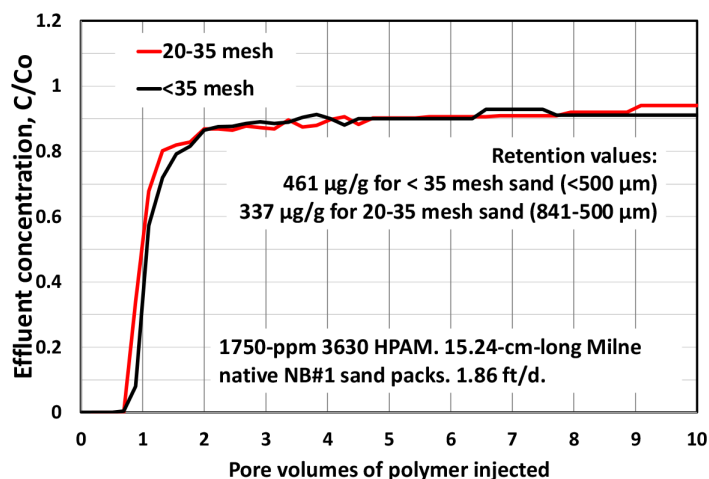


Fig. 5—Effect of particle size on tailing phenomenon in native NB1 sandpacks.

Effect of Sand Source, Polymer Concentration, and Molecular Weight. Another question was whether the tailing phenomenon depends on polymer concentration or molecular weight used for the retention study. This idea was tested by performing retention studies in native OA sandpacks, with concentrations of Flopaam 3630S ranging from 600 to 1,750 ppm. The results are shown in Fig. 6. The tailing phenomenon observed was quite similar to that observed in sandpacks using NB1 sand. Thus, the tailing phenomenon was seen in sand from two different Schrader Bluff sands (OA and NB) from the same well. Further, the shapes of the polymer breakout curves were very similar, regardless of polymer concentration (between 600- and 1,750-ppm Flopaam 3630S). The retention values for the three cases varied from 66 to 205 $\mu\text{g/g}$, primarily because polymer concentration weighs heavily in the retention calculation (see Eq. 1).

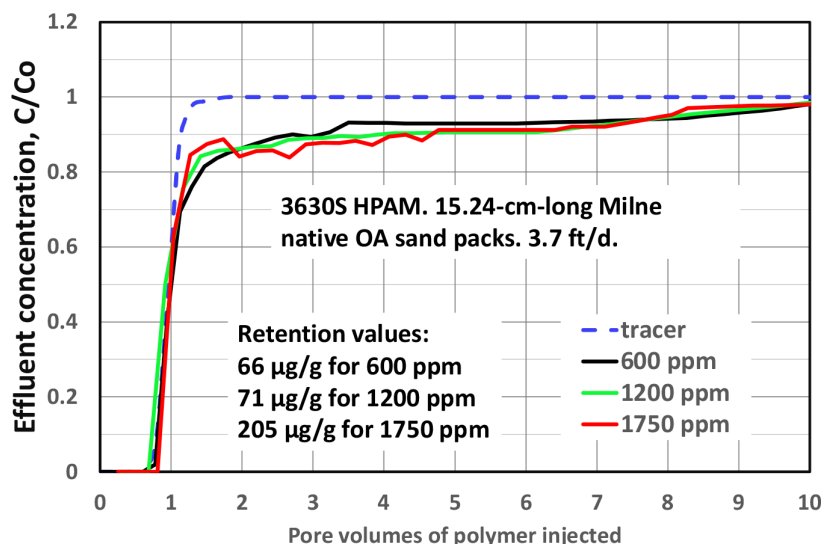


Fig. 6—Effect of polymer concentration on tailing phenomenon in native OA sandpacks.

Fig. 7 shows that a similar tailing effect occurred (in native OA sand) for 2,000-ppm Flopaam 3430S—a solution providing about the same polymer viscosity as 1,750-ppm 3630S, but using a lower-molecular-weight HPAM (11 million g/mol vs. 18 million g/mol). Polymer retention was about the same for the two cases (i.e., 236 $\mu\text{g/g}$ for 2,000-ppm 3430S vs. 205 $\mu\text{g/g}$ for 1,750-ppm 3630S). We acknowledge that one could attempt to make the comparison by performing experiments at identical molar polymer concentrations.

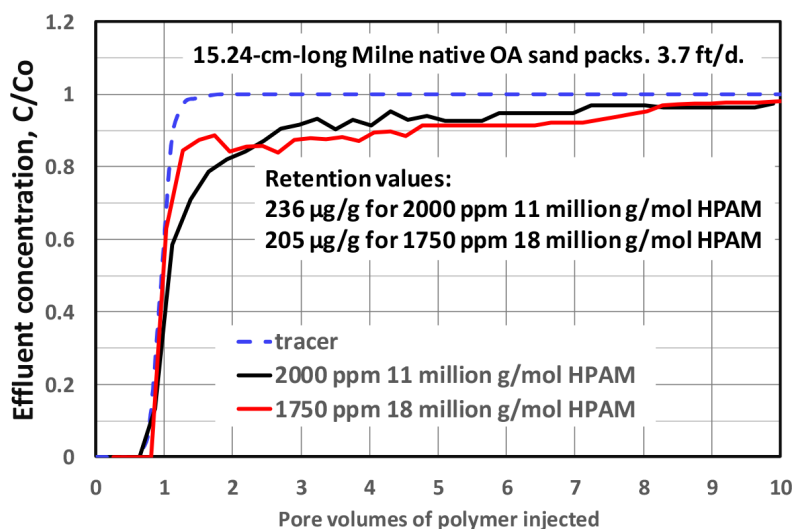


Fig. 7—Effect of polymer Mw on tailing phenomenon in native OA sandpacks.

Effect of Core Preservation State. A number of experiments were performed to determine whether the tailing phenomenon might be an artifact associated with how the core was preserved or restored. Fig. 8 shows that the tailing phenomenon was observed for a 6.7-cm-long preserved core from the Schrader Bluff NB sand. We also found tailing during retention studies in preserved OA cores. In previous work (Wang et al. 2020), tailing was noted in (1) native-state NB and OA sands, (2) cleaned (by extraction with toluene and methanol) NB and OA sands, (3) NB and OA sands that were cleaned and then resaturated with fresh Milne Point oil, and (4) cleaned, resaturated, and aged (at 60°C) NB cores. Combining this current work with the previous work, we note that the tailing phenomenon persisted in cores with different lengths (5.08–60 cm), permeabilities (50–6,108 md), and confinement pressures (100–1,750 psi).

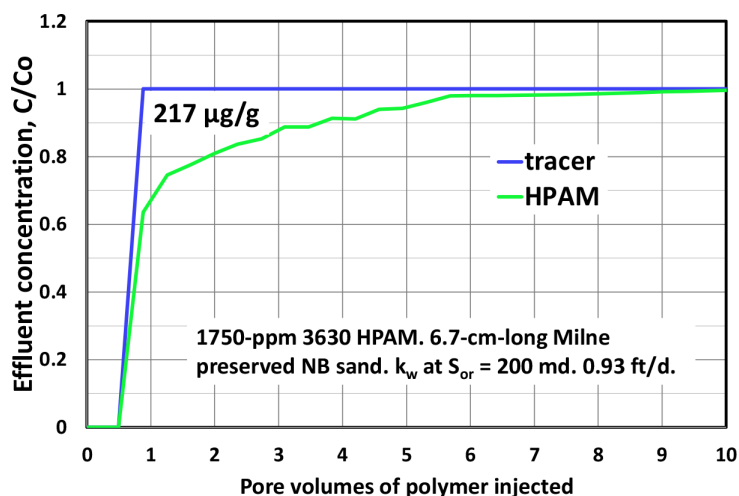


Fig. 8—Tailing phenomenon in a preserved NB sandpack.

Studies in Bead Packs with Known Additions of Selected Minerals

Particle-Size Distributions. Although the tailing phenomenon persists throughout these studies, we cannot yet identify a reason for its existence. Consequently, we performed a number of retention studies in “synthetic” packs of known composition—to examine how the tailing phenomenon depends on mineral composition. **Table 3** summarizes the properties of some of these packs. Our base-case for these studies involved injection of 1,750-ppm Flopaam 3630S into a 7-darcy pack of 200- μm glass beads (of very narrow size distribution). **Fig. 9** shows the particle-size distributions for these beads and for three Schrader Bluff sands. The mean particle size [Dv(50)] for the beads (212 μm) was reasonably close to that for the NB1 sand (166 μm). For the beads and each of the sands, various standard characterization parameters are listed in the table within **Fig. 9**. These parameters are defined in the Nomenclature. As seen in **Table 3**, a wide range of permeabilities were observed in these packs, depending on the mineral type and amount. Presumably, the observed permeabilities resulted from the amount, type, and particle-size distribution of the mineral involved.

Added Mineral	Permeability (md)	Polymer Retention ($\mu\text{g/g}$)	Tailing?
None (beads only)	7,000	0	No
2% CaSO_4	700	0	No
2% Kaolin	3,400	0	No
9% Kaolin	192	76	Yes
9% Illite	4,646	125	Yes
9% Chlorite	2,858	13	No
9% Montmorillonite	135	0	No
9% CaCO_3	938	186	No
5% CaCO_3	2,946	48	No
13% CaCO_3	1,378	162	No
9% FeCO_3	1,586	49	No
9% Dolomite	2,456	52	No
9% Pyrite	5,760	4	No

Table 3—Properties of packs with 200- μm beads and selected other minerals (no oil present) 1750-ppm HPAM (18 million g/mol Mw), 15.24 cm pack length, 1.86 ft/d darcy velocity.

Fig. A-1 in **Appendix A** plots particle-size distributions for four clays (illite, chlorite, kaolinite, and montmorillonite) that were used in this study. X-ray diffraction studies (Jones 2010; Rose et al. 2011; Wang et al. 2020) indicated that illite was commonly present in Milne Point core material—although a wide range of illite compositions were reported (1–21%). **Fig. A-2** plots size distributions for five other materials that were used in this study—limestone [CaCO_3], dolomite [$\text{CaMg}(\text{CO}_3)_2$], siderite [FeCO_3], pyrite (FeS_2), and CaSO_4 . All distributions in **Figs. A-1 and A-2** were very broad, usually with multiple peaks.

As shown in **Table 3**, in a 7-darcy bead pack (with no added minerals), polymer retention was zero and no tailing occurred. **Fig. 10** shows that the tailing phenomenon occurred to various extents with bead packs that contained 9% of the clays (kaolin, illite, and chlorite), with the remainder of the pack being the 200- μm beads. The 9% kaolin pack had a permeability of 192 md and exhibited retention of 76 $\mu\text{g/g}$. The 9% illite pack had a permeability of 4,646 md and exhibited a retention of 125 $\mu\text{g/g}$. The 9% chlorite pack had a permeability of 2,858 md and exhibited a retention of 13 $\mu\text{g/g}$. The retention and tailing for chlorite were not significant—perhaps because the particles of chlorite were larger than those of the other clays (blue curve in **Fig. A-1**).

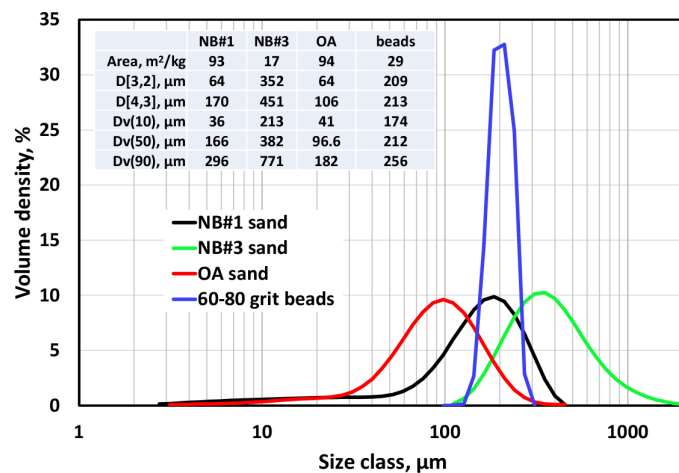


Fig. 9—Particle size distributions for glass beads vs. three sands.

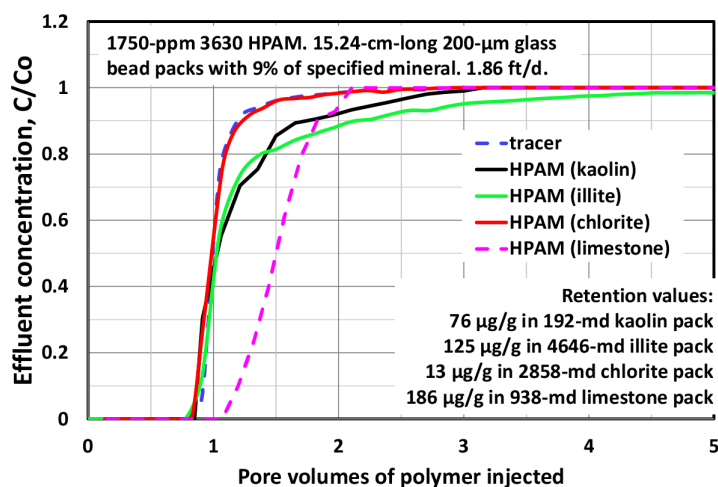


Fig. 10—Tailing phenomenon in bead packs with various minerals.

In contrast to illite and kaolin, a 938-md bead pack with 9% limestone exhibited polymer retention of 186 μg/g but showed no sign of tailing (dashed pink curve in Fig. 10). Additional bead pack studies with 5 and 13% limestone also showed no tailing, with retention values of 48 and 162 μg/g, respectively. No tailing phenomena were seen in bead packs with (1) 9% montmorillonite—which provided a 135-md pack and exhibited no retention, (2) 9% dolomite—which provided a 2,456-md pack and exhibited 52 μg/g retention, (3) 9% siderite—which provided a 1,586-md pack and exhibited 49 μg/g retention, (4) 9% pyrite—which provided a 5,760-md pack and exhibited 4 μg/g retention, and (5) 2% CaSO₄—which provided a 700-md pack and exhibited no polymer retention,

Thus, our results suggest that illite and kaolinite were the only minerals tested so far that exhibit the tailing phenomenon and might be the source of the tailing phenomenon in Milne Point cores. It is interesting that retention and tailing were not significant for the clays, montmorillonite, and chlorite and also for pyrite. No correlation is evident with permeability or grain size distribution.

Retention Studies in Bead Packs with Illite

Additional studies were performed with bead packs that contained illite, because (1) X-ray diffraction studies indicated that illite is the dominant clay present in Milne Point core material and (2) illite is one of the two minerals that definitively showed the tailing phenomenon.

Effect of Particle Size. To test how particle size affects polymer retention and tailing, we performed retention tests using three illite samples. The first sample was illite with the -particle-size distribution shown by the red curve in Fig. 11—where the median particle size was 330 μm. For the second and third illite samples, the first sample was sieved to produce a fraction that passed through 100 mesh (149 μm) and another fraction that passed through 20 mesh (841 μm) but was retained by 100 mesh. The second sample (through 100 mesh) had the particle-size distribution shown by the green curve in Fig. 11—where the median particle size was 29.3 μm. The third sample (between 20 and 100 mesh) had the particle-size distribution shown by the black curve in Fig. 11—where the median particle size was 509 μm. Note from the black curve that a small quantity of small particles was retained on the 100-mesh screen. The peaks for the small particles (at 0.6 and 5.2 μm) in the black curve were at least 20 times smaller than for the large peak (at 586 μm). The green curve had no particles larger than 300 μm. For comparison, the blue curve in Fig. 11 shows the particle-size distribution for the 200-μm glass beads.

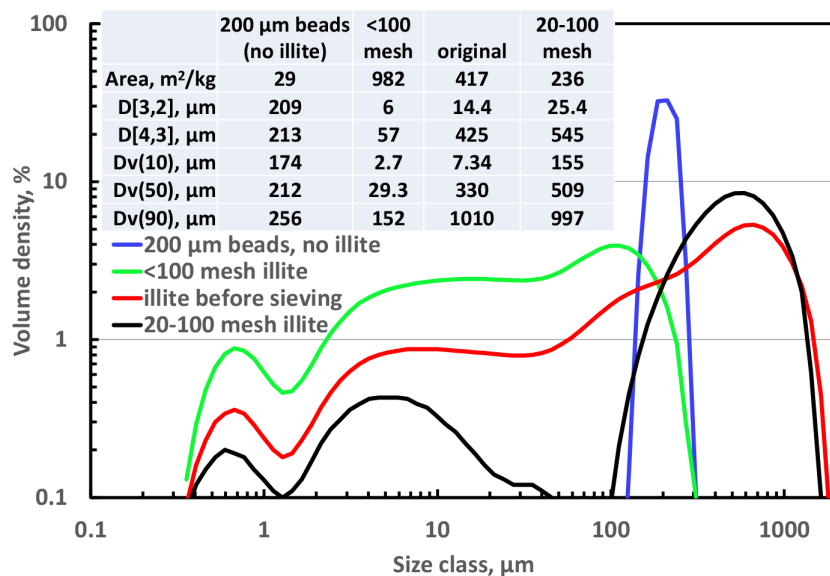


Fig. 11—Illite particle-size distributions before and after sieving.

Each of these three illite samples (from the same original source) was mixed with 200- μm glass beads—to make 9% illite in each of the three packs. Fig. 12 shows the results of the retention tests using the three illite samples, along with results using only the 200- μm beads (with no illite). Note that the three illite samples exhibited very similar tailing phenomena and retention values (117–125 $\mu\text{g}/\text{g}$). Close examination indicates that retention and tailing were very slightly greater as particle size decreased. However, for the most part, retention and tailing were apparently not sensitive to particle size or permeability (from 1,408 to 6,107 md). This finding is consistent with that observed for polymer retention in the Milne Point cores (Fig. 5).

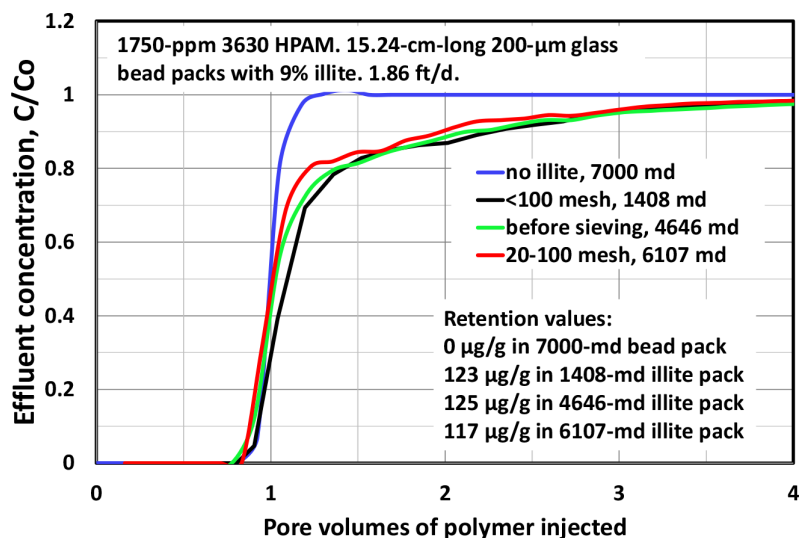


Fig. 12—Tailing phenomenon in 9% illite before vs. after sieving.

Effect of Flooding Rate. To test whether the tailing phenomenon is sensitive to flooding rate, two additional experiments were performed (using the illite that passed through 100 mesh) at 0.31 and 12.4 ft/d, respectively. Fig. 13 reveals that retention and tailing became modestly greater as the rate was decreased from 12.4 to 0.31 ft/d. The effect was most evident between 1 and 2 PV. Although the sensitivity to rate was not large, it appeared to be more definitive than was evident in the Milne Point cores (Fig. 3).

Effect of Polymer Molecular Weight, Concentration, and Anionicity. Figs. 6 and 7 suggest that the tailing was not sensitive to HPAM concentration (between 600 and 1,750 ppm) or Mw (between 11 and 18 million g/mol) in Milne Point core material. However, we were concerned that greater ranges of concentration and Mw were needed to properly investigate these effects. Consequently, additional retention studies were performed using SNF Flopaam 3,130 S (Mw ~2.7 million g/mol) and SNF Flodril TS705 (Mw ~0.3 million g/mol). All SNF polymer had 30% anionicity (degree of hydrolysis). We also tested Ciba Alcoflood 254 S (Mw ~0.1 million g/mol, 10% anionicity). The experiments were performed in bead packs with 9% illite (that was sieved through 100 mesh) using 1,750- and 200-ppm HPAM.

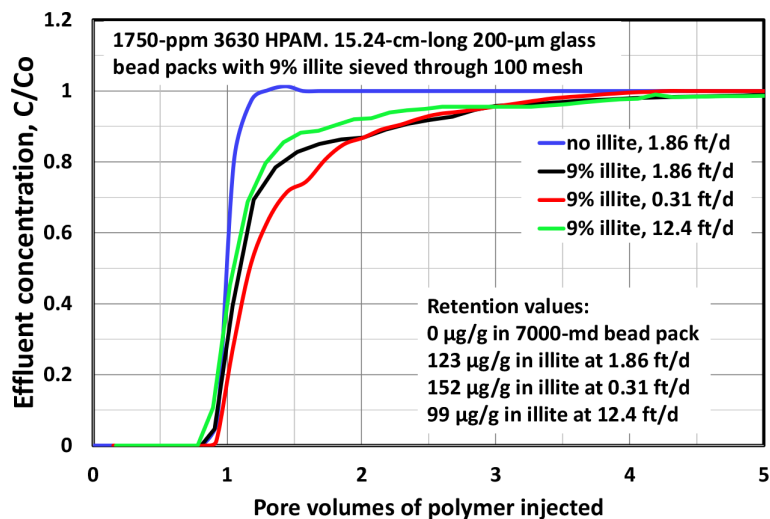


Fig. 13—Tailing phenomenon in 9% illite vs. flooding rate.

Comparison of the red and black solid and dashed curves in Fig. 14 reveals qualitatively similar behavior for the 2.7- and 18-million-g/mol polymers—except that the 2.7-million-g/mol HPAM exhibited less than half the retention—especially between 1 and 2.5 PV. Retention values for these cases are listed in Table 4.

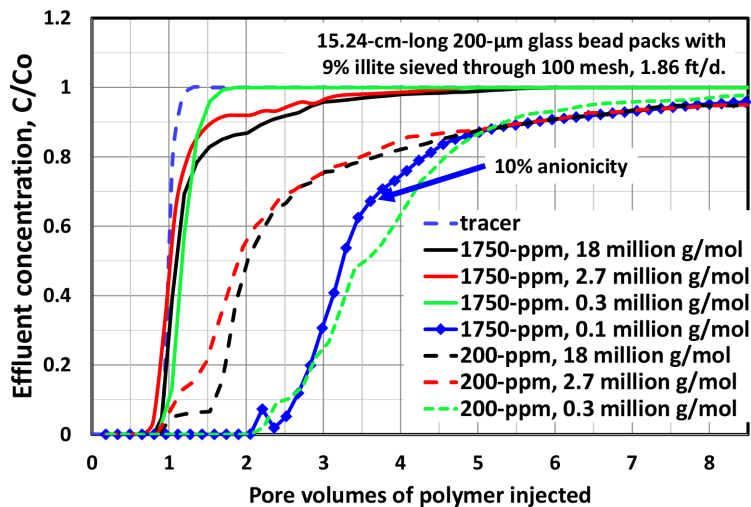


Fig. 14—Tailing phenomenon in 9% illite vs. HPAM molecular weight and concentration (30% anionicity).

Mw (10 ⁶ g/mol)	Anionicity (%)	HPAM (ppm)	Illite (%)	Illite Sieving	Rate (ft/d)	Length (cm)	Overall Retention (µg/g)	Retention, µg/g of illite
18	30	1,750	9	<100 mesh	0.31	15.24	152	1,672
18	30	1,750	9	<100 mesh,	1.86	15.24	123	1,353
18	30	1,750	9	<100 mesh,	12.4	15.24	99	1,089
18	30	200	9	<100 mesh	1.86	15.24	162	1,782
2.7	30	1,750	9	<100 mesh	1.86	15.24	53	583
2.7	30	200	9	<100 mesh	1.86	15.24	80	880
0.3	30	1,750	9	<100 mesh	1.86	15.24	71	781
0.3	30	200	9	<100 mesh	1.86	15.24	102	1,122
0.1	10	1,750	9	<100 mesh	1.86	15.24	972	10,692
18	30	1,750	9	No sieving	1.86	15.24	125	1,375
18	30	1,750	9	20–100 mesh	1.86	15.24	117	1,287

Table 4—Effect of various parameters for HPAM retention on illite (with 200-µm beads) (no oil present).

Mw (10 ⁶ g/mol)	Anionicity (%)	HPAM (ppm)	Illite (%)	Illite Sieving	Rate (ft/d)	Length (cm)	Overall Retention (μg/g)	Retention, μg/g of illite
18	30	1,750	9	20–100 mesh	1.86	30.48	69	759
18	30	1,750	9	20–100 mesh	1.86	61.00	100	1,100
18	30	1,750	4.5	20–100 mesh	1.86	15.24	3	66
18	30	1,750	18	20–100 mesh	1.86	15.24	133	732
18	30	1,750	36	20–100 mesh	1.86	15.24	209	575

Table 4 (continued)—Effect of various parameters for HPAM retention on illite (with 200-μm beads) (no oil present).

Interestingly, the 0.3 million-g/mol HPAM at 1,750-ppm (green solid curve) exhibited no tailing but a slight delay in initial polymer breakthrough (consistent with the Langmuir isotherm), yielding 71 μg/g retention. In contrast, the blue-diamond curve in Fig. 14 shows that the 0.1-million-g/mol polymer (10% anionicity) exhibited a substantial delay in polymer propagation. In this case, no polymer was produced until 2–2.5 PV. The solid red and black curves in Fig. 14 show that the higher-Mw (2.7 and 18 million g/mol) polymers (at 1,750 ppm) exhibited no delay in polymer breakthrough. This difference suggests that either the lowest-Mw HPAM (0.1 million g/mol) can penetrate deeper into the illite—leading to very high adsorption/retention (972 μg/g)—or that 10% anionicity causes substantially greater adsorption/retention than 30% anionicity. In contrast, the higher-Mw HPAMs appear largely unable to penetrate into the illite upon initial contact—resulting in significantly lower retention (53–123 μg/g). (Of course, a future study to decouple the effects of Mw from the degree of hydrolysis should be interesting. Also, a study of the behavior using different pH and salinity values could be interesting, because the surface charge of clay may depend on these parameters.)

Note that all (except the case of 0.3 million-g/mol HPAM at 1,750-ppm) polymers exhibit substantial tailing after polymer breakthrough (when 9% illite was present). This result suggests that even the lowest-Mw polymer (0.1 g/mol) experiences difficulty in penetrating into the tightest illite pores. For 200 ppm of the 2.7- and 18-million g/mol HPAMs (red and black dashed curves), the retention curves were notably below the red and black solid curves (1,750 ppm). The polymer concentration was at or below C^* for the red and black dashed curves and for the blue-diamond and green curves (see Table 1)—suggesting that the polymer more easily penetrates into the illite when the polymer concentration is at or below C^* . However, one could argue that the solid green curve (0.3 million g/mol at 1,750 ppm) might be an exception to this rule. Fig. 14 and Table 4 suggest a complicated relation between polymer retention on illite and polymer Mw, concentration, and anionicity.

Effect of Illite Content. To test how the tailing phenomenon depends on illite composition in the pack, additional experiments were performed (using the illite that passed through 20 mesh but was retained by 100 mesh). The illite content ranged from 4.5 to 36%, corresponding to pack permeabilities that ranged from 1,730 to 6,527 md. Fig. 15 shows the results. Very little retention (3 μg/g) was seen with 4.5% illite. The black dashed curve in Fig. 15 was quite similar to that for the KI tracer curve (not shown) for the 4.5%-illite case, and tailing was not particularly evident. In contrast, retention increased from 117 to 209 μg/g as illite content rose from 9 to 36%. The level of tailing became more pronounced also. In Fig. 15, the produced polymer concentrations departed from the KI-tracer curves at ~80% (of injected concentration) for 9% illite (green curve), ~70% for 18% illite (red curve), and ~50% for 36% illite (black solid curve). The produced polymer concentrations reached the injected values at ~4 PV for 9% illite, ~5 PV for 18% illite, and ~10 PV for 36% illite. These results suggest that the level of contact of polymer with illite was important. All cores visually appeared to have the illite uniformly distributed throughout the core—as judged by the color, texture, and core integrity. Of course, the illite could have experienced segregation on a subvisual level. However, if the illite was macroscopically segregated, the KI tracer breakout curves should have reflected this—via a noticeable tail in the KI breakout curves. In contrast, all KI tracer breakout curves for these cases were quite sharp (like the blue curves in Figs. 2 and 3)—indicating homogeneous cores. Further, as shown in Fig. 16, a plot of log of permeability vs. porosity (red data points and line) follows a consistent relation with changing illite content. If substantial segregation occurred for the

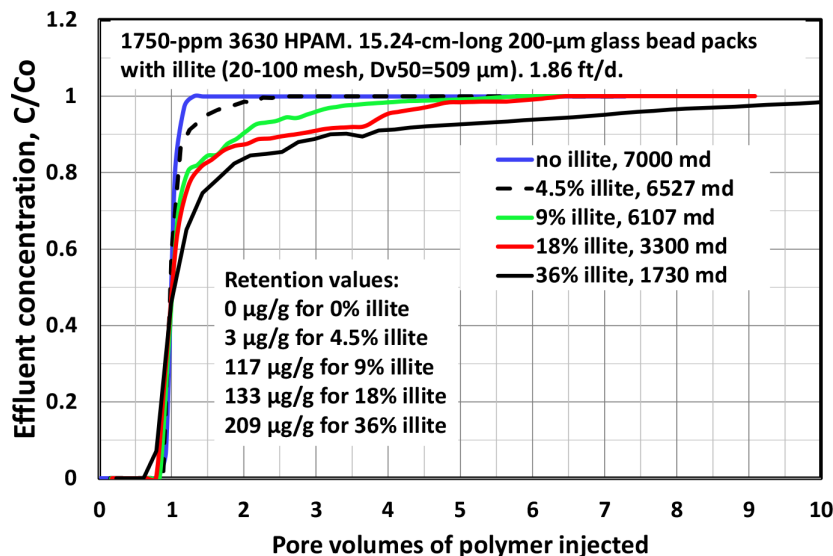


Fig. 15—Tailing phenomenon in 20–100-mesh illite vs. illite content in bead pack.

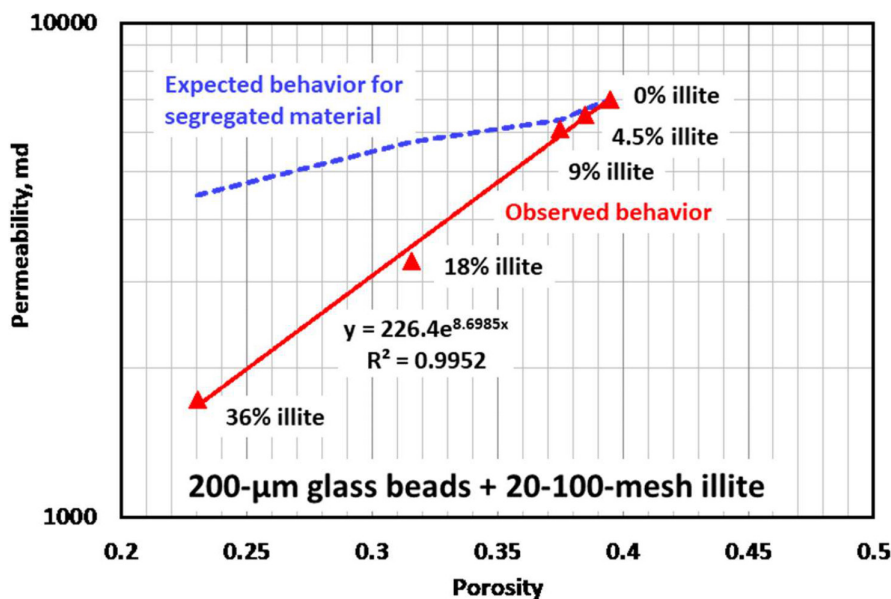


Fig. 16—Permeability-porosity relation vs. illite content.

beads and illite, one would have expected a substantial deviation for the plot in Fig. 16, as suggested by the blue dashed curve (which was calculated assuming Darcy's law for flow in parallel for totally segregated material).

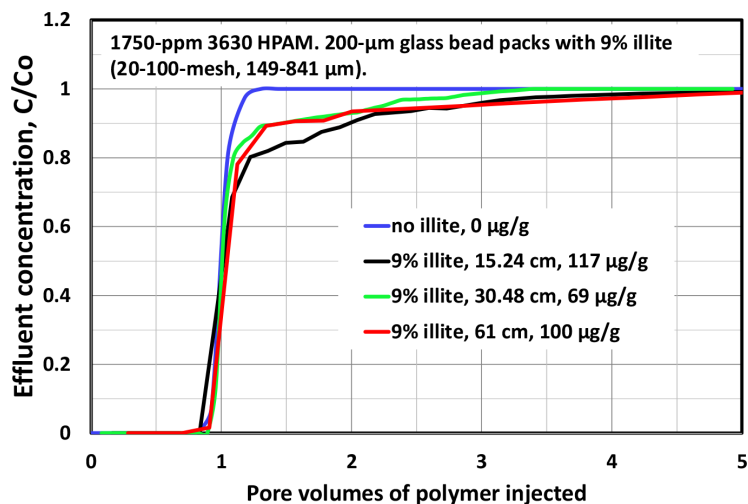


Fig. 17—Tailing phenomenon in 20–100-mesh illite vs. pack length.

We also performed an experiment that contained only 20–100-mesh illite (i.e., no glass beads). When subjected to 500 psi confining pressure, permeability to brine was only 0.4 md. Because of the low permeability, polymer injection was not attempted. Instead, we dried the pack and redetermined the particle-size distribution (red curve in Fig. A-3 in Appendix A)—to see if the process of compression (to 500 psi) affected particle size. Fig. A-3 illustrates that the compression process did indeed alter the illite size distribution—by significantly increasing the fraction of smaller illite particles. The black curve in Fig. A-3 shows the original particle-size distribution for illite, while the green curve shows the size distribution after sieving between 20 mesh (841 µm) and 100 mesh (149 µm). (This sieved material was used for the experiments in Figs. 12, 15, and 17.) Comparison with the red curve in Fig. A-3 indicates that the compression process produced small particles so that the low end of the size distribution (below 100 µm) matched that associated with the original unsieved illite (i.e., the black curve).

Effect of Pack Length. Using packs that contained 9% illite (20–100 mesh), Fig. 17 shows that the tailing phenomenon persisted for pack lengths from 15.24 to 61 cm. Although some variation was observed, the nature of the tailing was similar over this range of lengths—with total retention values from 69 to 117 µg/g. If the tailing was caused by channeling of the polymer through a pack (because of heterogeneity or uneven illite distribution along the pack), one would have expected the tailing to be mitigated as pack length increased. So, the behavior in Fig. 17 is consistent with our other observations indicating that the packs were all reasonably homogeneous—and the tailing was not because of uneven contact with illite within the packs.

Discussion

Surface Area/Particle Size. Electron micrographs of illite (Keller et al. 1986) show the surfaces to be quite rough. Polymer adsorption is expected to depend on the surface area of the adsorbing mineral. For a fixed weight of mineral, small particles will have a larger surface area than large particles. Consequently, one would expect polymer retention should be noticeably higher for packs with small particles than with large particles. In contrast, this concept does not receive much support from **Figs. 4 and 5** (for Milne Point core material) or from **Figs. 11 and 12** (for packs with 9% illite). Whatever is causing the tailing phenomenon seems to be fairly insensitive to particle size. However, as suggested by **Fig. A-3**, compression of the clay (e.g., to 500 psi) may have renormalized the illite size distribution to more closely match the original, unsieved clay. In that case, perhaps all our illite cases that were compressed actually had similar distributions of small illite particles. Also, the particle-size measurements were made under conditions where the particles were well-dispersed so that all grains had minimum contact with other particles. The extensive grain contact in compacted cores would substantially reduce the surface area that could contact the polymer.

Retention per Gram of Illite. For much of the above data for bead packs with illite, **Table 4** summarizes the results and (in the last column) expresses HPAM retention as μg per gram of illite. Previous calculations (summarized in the eighth column) included all solids (i.e., glass beads plus mineral) in the denominator of the retention calculation. If the results are excluded for the 4.5% illite case and the polymer with 10% anionicity, HPAM retention averaged 1100 μg of polymer per gram of illite—with variations extending from 575 to 1782 $\mu\text{g}/\text{g}$. Thus, it appears that for 9% illite and above, HPAM (with anionicity = 30%) retention (after many PV of polymer injection) is roughly 1100 $\mu\text{g}/\text{g}$ of illite, regardless of other conditions. However, from the last column of **Table 4**, we note that the average retention on illite that was sieved through 100 mesh ($<149 \mu\text{m}$) was generally higher than that for 20–100-mesh ($149\text{--}841 \mu\text{m}$) illite. This observation is consistent with the idea that smaller particles have a greater surface area and therefore should exhibit higher HPAM retention.

Proposed Model. In formulating a model for the retention tailing phenomenon, the model must account for the experimental observations mentioned previously. One can conceive of multiple mechanisms. Some mechanisms that could not adequately explain our experimental observations (e.g., polymer imbibition, flocculation, and IAPV) are discussed in **Appendix B**. This section will focus on the most applicable mechanism that we have examined to date. However, as will be seen, unanswered questions remain.

Much of the data (for HPAM with $M_w = 18$ million g/mol , 30% anionicity in packs with 9% illite) could be fitted using an “exposure parameter,” L_p , that is defined in Eq. 2:

$$L_p = (t - t_{bt})u C^{0.5}, \quad (2)$$

where t is the time since the start of polymer injection (seconds), t_{bt} is the time of first polymer arrival at the end of the core (seconds), u is the darcy velocity (cm/s), and C is the injected polymer concentration (weight fraction). The units for L_p are $\text{cm} \cdot (\text{wt. fraction})^{0.5}$. The effluent polymer concentration, relative to the injected value, C/C_o , was predicted quite well using Eq. 3:

$$C/C_o = 1 - 0.7e^{-L_p/0.03} - 0.3e^{-L_p/0.25}. \quad (3)$$

The red solid curve in **Fig. 18** reveals that this model described the observed behavior quite well for HPAM concentrations from 200 to 1,750 ppm, darcy velocities from 0.31 to 12.4 ft/d , pack lengths from 15.24 to 61 cm , and independent of illite particle size.

To rationalize this model, we note that polymer retention depends on the total time ($t - t_{bt}$) of polymer exposure to illite. This time difference is multiplied by the injection rate, u , to reflect that low rates cause longer exposure times for a given fluid element. This product is then multiplied by the square root of polymer concentration. One would expect that lower HPAM concentrations would show reduced reaction rates. However, the cause of the dependence on the square root of concentration is less obvious.

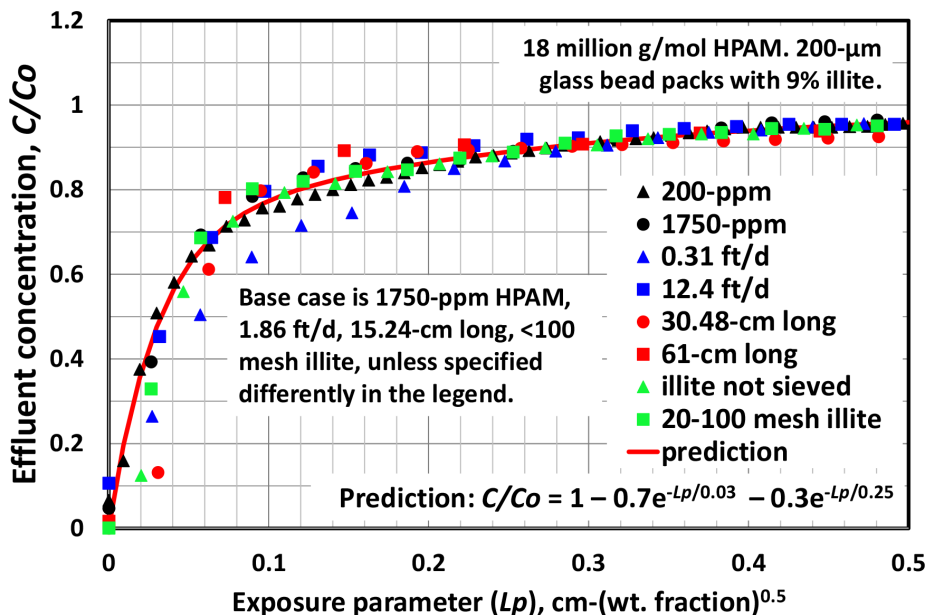


Fig. 18—Match of experimental data with the double-exponential model.

In Eq. 3, the two exponential terms suggest that two exposure-dependent processes occurred at the same time. The middle term reveals that ~70% of the concentration change was because of a relatively short process (with an exposure constant of 0.03), while the third term indicates that ~30% of the concentration change was ascribed to the longer process (with an exposure constant of 0.25). We understand the temptation to note the 0.3 multiplier and its similarity to the 20–30% inaccessible PV (IAPV) values that were sometimes reported in the literature (Manichand and Seright 2014). However, Appendix B presents arguments why the tailing phenomenon should be differentiated from IAPV. (In particular, IAPV accelerates polymer propagation through porous media, whereas the tailing phenomenon does not.) Also, we understand that Eq. 3 may require adjustment of the parameters for other polymer Mw values or illite concentrations. Consequently, additional work is needed.

Conceivably, the short process could be HPAM adsorption onto the outer (most accessible) surface of the illite, while the longer process could be associated with HPAM penetrating more deeply into the rough illite. To elaborate, illite is known to be a layered structure where an alumina layer is tightly bound between two silica layers, which in turn are loosely bound to other layers. One might speculate that HPAM intercalates between the loosely bound layers to explain the tailing process. A problem with this logic is that intercalation of HPAM between illite layers should expand the clay, leading to clay swelling and subsequent permeability reduction of the porous medium. This plugging/permeability reduction was never observed with any of our experiments with illite.

Another possibility is that HPAM adsorption occurs only on the outer surface of the illite, but that two separate types of adsorption sites exist with different adsorption characteristics—causing the double exponential in Eq. 3. Additional work is needed to understand the tailing phenomenon.

Relevance to Field Results

Credible prediction of the performance of a polymer flood requires an accurate characterization of oil mobilization, which in turn requires an appropriate representation of polymer retention and propagation through the reservoir. As mentioned earlier, the standard Langmuir isotherm in simulators and the standard assumption of concentration-independent retention in fractional flow calculations cannot correctly describe polymer retention at the Milne Point polymer flood. Our findings suggest a similar concern for any polymer flood where significant levels of illite or kaolinite are present in the reservoir. Mineralogy analysis (especially for kaolinite and illite) is strongly encouraged to reveal whether the tailing phenomenon should be accounted for during simulations of polymer propagation/retention in a given field application.

At the Milne Point polymer flood, HPAM was first detected in both horizontal production wells (J-27 and J-28) after injecting only 10% PV (Dandekar et al. 2021). On the one hand, the fast polymer breakthrough is consistent with our experimental results in the sense that no delay in polymer propagation is evident because of retention. Also consistent with the experimental results, the maximum produced polymer concentration to date is 48% (in J-27) and 59% (in J-28) of the injected concentration. On the other hand, the fast polymer breakthrough is probably because of channeling through a fracture-like feature, rather than via propagation through typical Schrader Bluff reservoir sand. Given the near-unit-mobility displacement provided by the injected polymer solutions, breakthrough would not be expected before injection of 50% PV polymer solution. Thus, definitive field confirmation of the tailing effect will require significant additional time, PV injected, and analysis of produced polymer. As mentioned earlier, we anticipate that the tailing behavior should result in no significant delay in propagation of the polymer bank (and therefore the oil bank), but the effective viscosity and displacement efficiency may be less than originally planned. To reiterate a very positive note, produced water cuts dropped from ~70% during waterflooding before the project to less than 10% during polymer injection. To our knowledge, no other field polymer flood has resulted in this magnitude of reduction in water-cut. At this time, only 15% PV of the polymer has been injected, so there certainly is no delayed response to polymer injection.

Because this polymer flood is still in its relatively early stages and because a number of factors influence the current produced polymer concentrations, we cannot yet make definitive conclusions about the actual polymer retention that has occurred within the Milne Point field. Properly assessing retention on a field scale will require significantly more time, polymer throughput, and a methodology like that in Manichand and Seright (2014).

Conclusions

1. Laboratory retention studies for the Milne Point polymer flood (North Slope of Alaska) consistently show virtually no delay in polymer propagation, a rapid rise in produced polymer to 70–90% of the injected concentration, followed by produced concentration gradually approaching the injected value over many PV.
2. In contrast, conventional use of the Langmuir isotherm (used in most chemical flooding simulators) or concentration-independent polymer retention (used during fractional-flow calculations) predicts a delay in propagation of the polymer front (in proportion to the given retention value), followed by a rapid rise in produced polymer concentration to the injected level.
3. From a practical viewpoint, this tailing behavior means that retention causes no significant delay in propagation of the polymer bank (and therefore the oil bank), but the effective viscosity and displacement efficiency are less than originally planned.
4. In Milne Point cores, over practical ranges of conditions encountered in the field, the presence of the tailing phenomenon was not sensitive to flow rate, polymer concentration, core heterogeneity, or whether the core was preserved, cleaned of oil, or cleaned and resaturated with oil, or cleaned, resaturated, and aged with oil.
5. The tailing phenomenon was also observed during mechanistic floods using glass bead packs when sufficient levels of kaolinite or illite were present. This observation was consistent with high levels of illite noted in Milne Point cores.
6. The tailing phenomenon was not noted during mechanistic floods that contained glass beads with montmorillonite, chlorite, calcium carbonate, dolomite, siderite, pyrite, or calcium sulfate.
7. The work suggests that mineralogy analysis (especially for kaolinite and illite) may reveal whether the tailing phenomenon should be accounted for during simulations of polymer propagation/retention in a given field application.
8. A model was proposed to account for the retention tailing phenomenon. Much of the retention data could be fitted to a double-exponential equation, where a relative short reaction accounted for ~70% of the HPAM retention and a longer reaction accounted for the remaining ~30%. Additional work is needed to elucidate the mechanism associated with the tailing mechanism.

Nomenclature

- A_p = particle area, μm^2
 C = effluent concentration, mg/L or ~ppm ($\mu\text{g/g}$)
 C_o = injected concentration, mg/L or ~ppm ($\mu\text{g/g}$)

- C_p = effluent polymer concentration, mg/L or ~ ppm ($\mu\text{g/g}$)
 C_{po} = injected polymer concentration, mg/L or ~ ppm ($\mu\text{g/g}$)
 C_t = effluent tracer concentration, mg/L or ~ ppm ($\mu\text{g/g}$)
 C_{to} = injected tracer concentration, mg/L or ~ ppm ($\mu\text{g/g}$)
 C^* = polymer critical overlap concentration, mg/L or ~ ppm ($\mu\text{g/g}$)
 d_s = surface diameter, $(A_p/\pi)^{1/2}$, μm
 d_v = volume diameter, $(6V_p/\pi)^{1/3}$, μm
 $D[3,2]$ = Sauter mean diameter, d_v^3/d_s^2 , μm
 $D[4,3]$ = d_v^4/d_s^3 , μm
 $Dv(10)$ = particle diameter below which accounts for 10% of the material volume, μm
 $Dv(50)$ = particle diameter below which accounts for 50% of the material volume, μm
 $Dv(90)$ = particle diameter below which accounts for 90% of the material volume, μm
 $IAPV$ = inaccessible pore volume
 k = permeability, darcies (μm^2)
 k_{wsor} = permeability to water at residual oil saturation, darcies (μm^2)
 L_p = exposure parameter in Eqs. 2 and 3, cm-(wt. fraction)^{0.5}
 M_{rock} = mass of rock in the sandpack, g
 Mw = polymer molecular weight, g/mol (daltons)
 PV = pore volumes of fluid injected
 q_{gmb} = imbibition rate, cm^3/h
 R_{pret} = polymer retention, $\mu\text{g/g}$
 S_{or} = residual oil saturation
 t = time, seconds
 t_{bt} = polymer breakthrough time in Eq. 2, seconds
 u = darcy velocity, cm/s
 V_p = particle volume, μm^3
 ΔPV = pore volumes difference
 Δt = incremental time, hours
 ΔV = incremental effluent volume, cm^3
 ϕ = porosity
 ρ_{rock} = rock density, g/cm^3

Disclaimer

This report was prepared as an account of work sponsored by an agency of the United States Government. Neither the United States Government nor any agency thereof, nor any of their employees, makes any warranty, express or implied, or assumes any legal liability or responsibility for the accuracy, completeness, or usefulness of any information, apparatus, product, or process disclosed, or represents that its use would not infringe privately owned rights. Reference herein to any specific commercial product, process, or service by trade name, trademark, manufacturer, or otherwise does not necessarily constitute or imply its endorsement, recommendation, or favoring by the United States Government or any agency thereof. The views and opinions of authors expressed herein do not necessarily state or reflect those of the United States Government or any agency thereof.

Acknowledgments

We thank Baojun Bai, Abhijit Dandekar, Samson Ning, Brent Sheets, Yin Zhang, and the rest of the team associated with Department of Energy Award Number DE-FE0031606 for interesting discussions. Thanks also to Hilcorp for providing the oil and core material used in this work. We are also grateful to SNF for providing the polymers. Thanks also to Orval Seright, Marie Gibbons, and Dr. Lloyd Berg for greatly appreciated guidance and help.

"This material is based upon work supported by the Department of Energy under Award Number DE-FE0031606."

References

- Chang, H., Zhang, Y., Dandekar, A. Y. et al. 2020. Experimental Investigation on Separation Behavior of Heavy-Oil Emulsion for Polymer Flooding on Alaska North Slope. *SPE Prod & Oper* **35** (3): 579–591. SPE-200369-PA. <https://doi.org/10.2118/200369-PA>.
- Dandekar, A., Bai, B., Barnes, J. et al. 2020. First Ever Polymer Flood Field Pilot to Enhance the Recovery of Heavy Oils on Alaska's North Slope - Pushing Ahead One Year Later. Paper presented at the SPE Western Regional Meeting, Bakersfield, California, USA, 27 April–1 May. SPE-200814-MS. <https://doi.org/10.2118/200814-MS>.
- Dandekar, A., Bai, B., Barnes, J. et al. 2019. First Ever Polymer Flood Field Pilot - A Game Changer to Enhance the Recovery of Heavy Oils on Alaska's North Slope. Paper presented at the SPE Western Regional Meeting, San Jose, California, USA, 23–26 April. SPE-195257-MS. <https://doi.org/10.2118/195257-MS>.
- Dandekar, A., Bai, B., Barnes, J. et al. 2021. Heavy Oil Polymer EOR in the Challenging Alaskan Arctic - It Works! Paper presented at the SPE/AAPG/SEG Unconventional Resources Technology Conference, Houston, Texas, USA, 26–28 July. URTEC-2021-5077-MS. <https://doi.org/10.15530/urtec-2021-5077>.
- Dawson, R. and Lantz, R. B. 1972. Inaccessible Pore Volume in Polymer Flooding. *SPE J.* **12** (5): 448–452. SPE-3522-PA. <https://doi.org/10.2118/3522-PA>.
- Dhaliwal, A., Zhang, Y., Dandekar, A. Y. et al. 2021. Experimental Investigation of Polymer-Induced Fouling of Heater Tubes in the First-Ever Polymer Flood Pilot on Alaska North Slope. *SPE Prod & Oper* **36** (1): 70–82. SPE-200463-PA. <https://doi.org/10.2118/200463-PA>.
- Ferreira, V. H. S. and Moreno, R. B. Z. L. 2020. Polyacrylamide Adsorption and Readsorption in Sandstone Porous Media. *SPE J.* **25** (1): 497–514. SPE-199352-PA. <https://doi.org/10.2118/199352-PA>.
- Gil, L., Gaillard, N., and Favero, C. 2015. Qualitative Determination of Polymer Presence by Flocculation. SNF Procedure QC-5065A.
- Green, D. W. and Willhite, G. P. 2018. *Enhanced Oil Recovery*, Second edition. Richardson, Texas, USA: Textbook Series, Society of Petroleum Engineers.

Guetni, I., Marliere, C., Rousseau, D. et al. 2019. Transport of HPAM Solutions in Low Permeability Porous Media: Impacts of Salinity and Clay Content. Paper presented at the SPE Europec Featured at 81st EAGE Conference and Exhibition, London, England, UK, 3–6 June. SPE-195434-MS. <https://doi.org/10.2118/195434-MS>.

Horne, R. N. and Rodriguez, F. 1983. Dispersion in Tracer Flow in Fractured Geothermal Systems. *Geophys Res Lett* **10** (4): 289–292. <https://doi.org/10.1029/GL010i004p00289>.

Jones, C. A. 2010. *Engineering Properties of Resedimented Ugnu Clay from the Alaskan North Slope*. Master of Science in Civil and Environmental Engineering Thesis, Massachusetts Institute of Technology.

Jouenne, S. and Levasche, B. 2020. Universal Viscosifying Behavior of Acrylamide-Based Polymers Used in Enhanced Oil Recovery. *J Rheol* **64** (5): 1295–1313. <https://doi.org/10.1122/8.0000063>.

Keller, W. D., Reynolds, R. C., and Inoue, A. 1986. Morphology of Clay Minerals in the Smectite-to-Illite Conversion Series by Scanning Electron Microscopy. *Clays Clay Miner* **34** (2): 187–197. <https://doi.org/10.1346/CCMN.1986.0340209>.

Ma, S. M., Zhang, X., Morrow, N. R. et al. 1999. Characterization of Wettability From Spontaneous Imbibition Measurements. *J Can Pet Technol* **38** (13): PETSOC-99-13-49. <https://doi.org/10.2118/99-13-49>.

Manichand, R. N. and Seright, R. S. 2014. Field vs. Laboratory Polymer-Retention Values for a Polymer Flood in the Tambaredjo Field. *SPE Res Eval & Eng* **17** (3): 314–325. SPE-169027-PA. <https://doi.org/10.2118/169027-PA>.

Mattax, C. C. and Kyte, J. R. 1962. Imbibition Oil Recovery from Fractured, Water-Drive Reservoir. *SPE J.* **2** (2): 177–184. SPE-187-PA. <https://doi.org/10.2118/187-PA>.

Ning, S., Barnes, J., Edwards, R. et al. 2019. First Ever Polymer Flood Field Pilot to Enhance the Recovery of Heavy Oils on Alaska’s North Slope - Polymer Injection Performance. Paper presented at the SPE/AAPG/SEG Unconventional Resources Technology Conference, Denver, Colorado, USA, 22–24 July. URTEC-2019-643-MS. <https://doi.org/10.15530/urtec-2019-643>.

Perkins, T. K. and Johnston, O. C. 1963. A Review of Diffusion and Dispersion in Porous Media. *SPE J.* **3** (1): 70–84. SPE-480-PA. <https://doi.org/10.2118/480-PA>.

Rose, K., Boswell, R., and Collett, T. 2011. Mount Elbert Gas Hydrate Stratigraphic Test Well, Alaska North Slope: Coring Operations, Core Sedimentology, and Lithostratigraphy. *Mar Pet Geol* **28** (2): 311–331. <https://doi.org/10.1016/j.marpetgeo.2010.02.001>.

Seright, R. S. 2017. How Much Polymer Should Be Injected During a Polymer Flood? Review of Previous and Current Practices. *SPE J.* **22** (1): 1–18. SPE-179543-PA. <https://doi.org/10.2118/179543-PA>.

Sugar, A., Serag, M., Torrealba, V. A. et al. 2021. Visualization of Polymer Retention Mechanisms in Porous Media Using Microfluidics. Paper presented at the SPE Europec 82nd EAGE Conference and Exhibition, Amsterdam, The Netherlands, 14–17 June. SPE 200557. <https://doi.org/10.2118/200557-MS>.

Wang, D., Li, C., and Seright, R. S. 2020. Laboratory Evaluation of Polymer Retention in a Heavy Oil Sand for a Polymer Flooding Application on Alaska’s North Slope. *SPE J.* **25** (4): 1842–1856. SPE-200428-PA. <https://doi.org/10.2118/200428-PA>.

Wang, D., Namie, S., and Seright, R. S. 2022. Pressure Barrier Applicability to Polymer Flood Design. Paper presented at the SPE Virtual Improved Oil Recovery Conference, Tulsa, Oklahoma, USA, 25–29 April. SPE-209462-MS. <https://doi.org/10.2118/209462-MS>.

Wang, D., Zhang, J., Butler, R. et al. 2016. Scaling Laboratory-Data Surfactant-Imbibition Rates to the Field in Fractured-Shale Formations. *SPE Res Eval & Eng* **19** (3): 440–449. SPE-178489-PA. <https://doi.org/10.2118/178489-PA>.

Wever, D. A., Bartlema, H., ten Berge, A. B. et al. 2018. The Effect of the Presence of Oil on Polymer Retention in Porous Media from Clastic Reservoirs in the Sultanate of Oman. Paper presented at the SPE EOR Conference at Oil and Gas West Asia, Muscat, Oman, 26–28 March. SPE-190430-MS. <https://doi.org/10.2118/190430-MS>.

Yang, Y., Liu, T., Li, Y. et al. 2021. Effects of Velocity and Permeability on Tracer Dispersion in Porous Media. *Appl Sci* **11** (10): 4411. <https://doi.org/10.3390/app11104411>.

Zhang, G. and Seright, R. S. 2014. Effect of Concentration on HPAM Retention in Porous Media. *SPE J* **19** (3): 373–380. SPE-166265-PA. <https://doi.org/10.2118/166265-PA>.

Zhao, Y., Yin, S., Seright, R. S. et al. 2021. Enhancing Heavy-Oil-Recovery Efficiency by Combining Low-Salinity-Water and Polymer Flooding. *SPE J.* **26** (3): 1535–1551. SPE-204220-PA. <https://doi.org/10.2118/204220-PA>.

Appendix A—Particle-Size Distributions

This appendix shows particle-size distributions for materials mentioned in the main body of the paper.

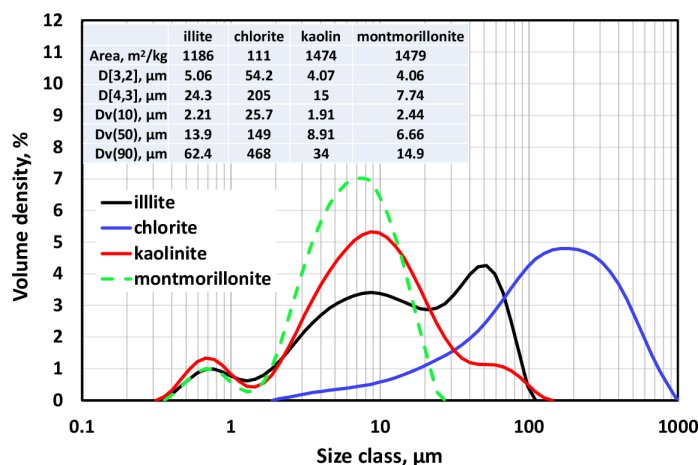


Fig. A-1—Particle-size distributions for four clays.

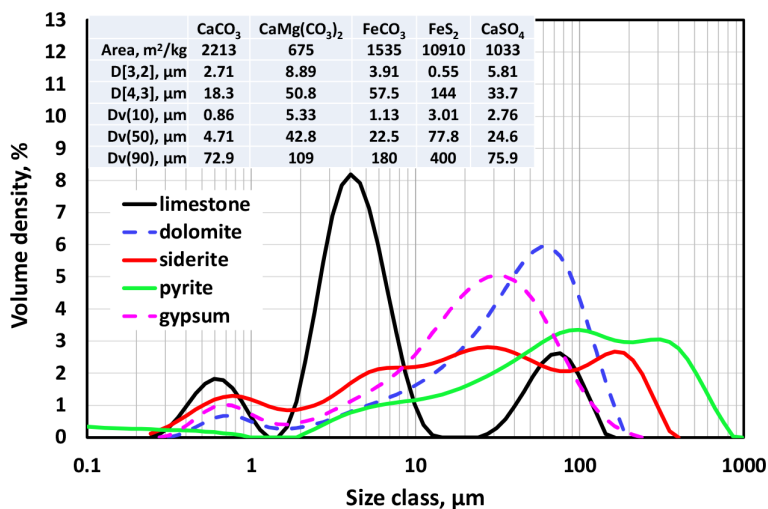


Fig. A-2—Particle-size distributions for five mineral additives.

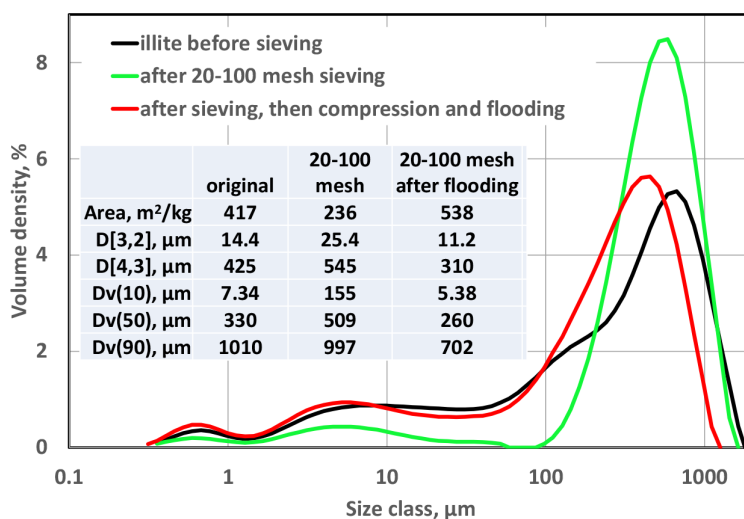


Fig. A-3—Illite particle-size distributions before and after compression and flooding.

Appendix B—Inadequate Mechanisms

This appendix describes mechanisms that were examined but could not adequately explain the experimental observations.

HPAM Imbibition into Illite. We considered the possibility of polymer imbibition into the clay as an explanation for the tailing phenomenon. [Some previous papers on the imbibition process for oil, water, and/or surfactant include Mattax and Kyte (1962), Ma et al. (1999), and Wang et al. (2016).] In our cases with illite in the 200- μm bead packs **Figs. 12, 13, 15, and 17**, we estimated the rate of polymer solution imbibition into the illite by assuming that all HPAM retention (after polymer breakthrough) was attributed to polymer-solution imbibition into the clay. Consequently, for a given increment of effluent volume (ΔV), the rate of polymer-solution imbibition (q_{imb}) was given by Eq. B-1:

$$q_{imb} = \Delta V [(C_t/C_{t0}) - (C_p/C_{p0})] / \Delta t, \quad (\text{B-1})$$

where C_t/C_{t0} is the effluent tracer concentration relative to the injected tracer concentration, C_p/C_{p0} is the effluent polymer concentration relative to the injected polymer concentration, and Δt is the time increment during the collection of that effluent sample. **Fig. B-1** shows the results of these calculations associated with the data in **Figs. 12, 13, and 17**. For a given curve, the rapid decline in imbibition rate with time could be rationalized as substantial increases in resistance to flow as the high-molecular-weight polymer attempts to penetrate further into the very small pores associated with the 0.4-md illite. However, many other observations are more difficult to explain using an imbibition model.

The three black curves in **Fig. B-1** reveal that the apparent rate of polymer imbibition into illite did not depend on the illite particle size. However, as discussed earlier, it is possible that the compression process (i.e., adding the 500 psi confining pressure) so that the particle-size distributions were effectively the same for these three cases.

The black, green, and red curves with triangles in **Fig. B-1** show that the apparent imbibition rate was not sensitive to pack length (between 15.24 and 61 cm). This finding is counterintuitive because the total illite surface area is proportional to pack length. So, one would expect the imbibition rate (in cm^3/h at a given exposure time) to be four times as high for the 61-cm pack as for the 15.24-cm pack.

The light blue, black, and dark blue curves with circles in **Fig. B-1** show that the apparent imbibition rate increased substantially with an increased flood rate between 0.31 and 12.4 ft/d. In fact, the curves in **Fig. B-1** could be almost be made to coincide if the time scale was divided by the flood rate raised to the 2/3 power. This finding is also counterintuitive because one would expect the rate of polymer imbibition into the clay to be insensitive to the fluid velocity outside of the clay (assuming other conditions are fixed).

Fig. B-2 shows the effect of illite concentration in the bead packs (between 4.5 and 36%). All cases here used 1.86 ft/d flood rate, were 15.24 cm long, and used 20–100-mesh illite. If the imbibition model was valid, we expected that the y -axis in **Fig. B-2** should be normalized by plotting the imbibition rate per gram of illite (i.e., $\text{cm}^3/(\text{h-g-illite})$). However, **Fig. B-2** does not reveal an understandable relation between apparent imbibition rate with illite content in the pack.

In summary, the imbibition model does not provide a satisfactory explanation for the tailing phenomenon.

Flocculation. Clays are known to flocculate with certain clays. In fact, flocculation with kaolinite is a common (although not necessarily reliable) method to detect HPAM in polymer production wells (Gil et al. 2015; Wang et al. 2020). Because our illite was added as loose powder to the 200- μm beads, some illite particles may have become suspended in the flowing liquid during the flooding process—and subsequently flocculated with the HPAM. However, if this was a significant occurrence, one would expect pressures to increase substantially during flocculation (because of filtration of the flocculated clay within the bead pack). In contrast, for all floods described in this paper, no external or internal plugging was observed during polymer flooding. For a fixed injection rate, injection pressures always increased rapidly (within about 1 PV) to the maximum value (at polymer breakthrough) that was not exceeded during the remainder of the multipore-volume injection process. Thus, clay flocculation with polymer does not appear to be responsible for the tailing phenomenon.

Inaccessible Pore Volume. Upon initial consideration, one might wonder if the tailing phenomenon is because of IAPV. However, more detailed consideration casts doubt on this suggestion.

A tailing phenomenon is often seen when a water tracer is continuously injected into a heterogeneous core (Perkins and Johnston 1963; Horne and Rodriguez 1983; Yang et al. 2021). In a homogeneous core or sandpack, the pathways through the porous medium are randomized, so no particular pathway has much preference over another. Consequently, the tracer arrives at the end of the core and rises to match the injected concentration in a fairly sharp manner—like the blue curves in **Figs. 2, 3, 6, 8, 10, and 14**. In contrast, in a heterogeneous porous medium, the tracer will arrive in the effluent early by traveling through the most direct and permeable pathway. After breakthrough, tracer from less-permeable pathways will arrive in the effluent at different times—thus giving the appearance of a concentration tail. Because our water tracer curves always gave sharp breakout curves, our cores and sand packs were homogeneous. Also, for the bead

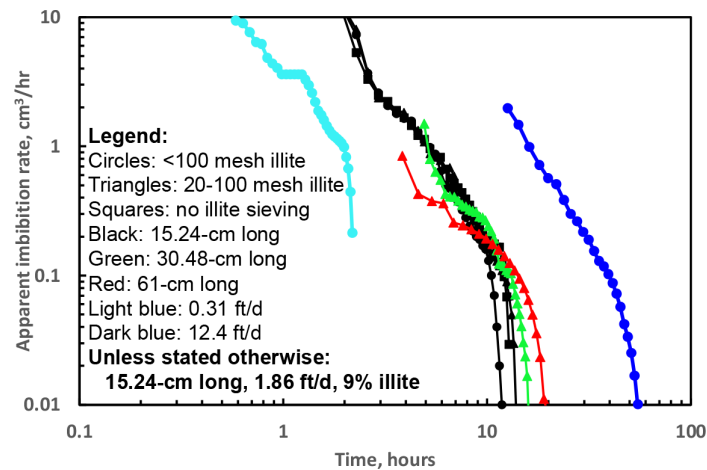


Fig. B-1—Calculated imbibition into illite using Eq. 2 and **Figs. 12, 13, and 17**.

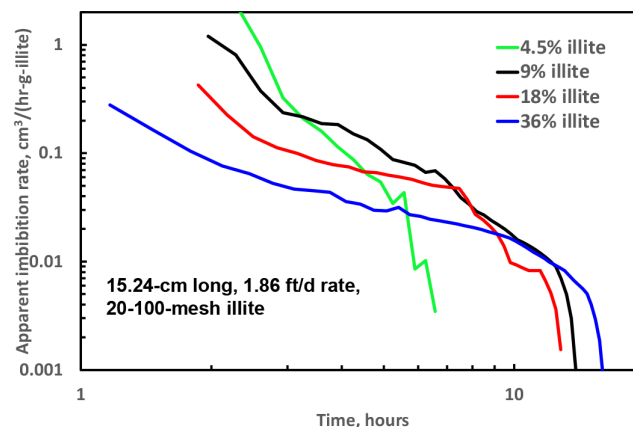


Fig. B-2—Calculated imbibition into illite using Eq. 2 and **Fig. 15** (effect of illite content).

packs, the coloration and shading given by various additives suggested that the packs had no obvious heterogeneity (e.g., separation between the 200 μm beads and the added mineral). Nevertheless, it is conceivable that the polymer saw heterogeneity as it propagated through the core, even though the tracer did not. IAPV might be viewed as such a phenomenon (Dawson and Lantz 1972; Manichand and Seright 2014; Wang et al. 2020). It is conceivable that the KI tracer can freely flow through the illite but the high molecular-weight polymer has limited access.

We used the PV associated with the tracer breakout as the primary basis of porosity in our analysis. One might think that if a certain fraction (e.g., 9, 18, and 36%) of clay is present, then there must be a large fraction of very small pores that are “inaccessible” to the polymer. Admittedly, extremely small pores may exist in the clays, but if the water tracer (iodide) is not “seeing” that porosity, we feel justified in not considering it as part of our practical porosity—just as is the normal case in reservoir engineering where rock with permeability/porosity that is below a certain value is excluded from the “net-pay.”

Next, the reader should note several key findings reported in Manichand and Seright (2014) and Wang et al. (2020). Manichand and Seright (2014) examined IAPV over the past 50 years and noted no logical correlation between IAPV, permeability, and polymer molecular weight. That does not negate the possibility of IAPV (especially, in tight rock), but it suggests that an important experimental difficulty may challenge the correct measurement of IAPV. Wang et al. (2020) demonstrated that viscous fingering associated with insufficient brine post-flush (after the polymer) leads to a substantial over estimation of IAPV. Seright (2017) and Wang et al. (2020) noted that most previous literature reports of IAPV either used small/insufficient brine post-flushes (i.e., 10 PV or less) or did not report the volume associated with the brine post-flush. Wang et al. (2020) out that variable or insufficient post-flushes could account for the inconsistent results reported for IAPV in the literature. Basically, one could obtain virtually any desired IAPV simply by adjusting the brine post-flush volume. Second, (as argued in Manichand and Seright 2014) comparison of polymer molecular sizes with permeabilities/pore sizes in the most significant field applications (i.e., >200 md) suggests that HPAM polymers are small enough to penetrate effectively into the vast majority of pores (e.g., $>99\%$) that are of practical significance in these polymer floods. We acknowledge that carbonates and other tight rocks may have smaller pores that really are inaccessible to HPAM, but that is not the case for the Milne Point sand—and probably not for other major floods, like Daqing, Mangala, Pelican Lake, etc.

In reviewing the previous literature on IAPV (Manichand and Seright 2014), the reported IAPV is seen as an acceleration of the polymer propagation through the porous medium. In contrast, for the tailing phenomenon examined in this paper, the polymer always arrives at the core outlet at the same time as the tracer. Rather than materializing as an acceleration of polymer propagation (as argued by most proponents of IAPV), the tailing phenomenon clearly exhibits a delay in propagation for part of the polymer. Also, as revealed in Wang et al. (2020), tests of intrinsic viscosity and dynamic light scattering of the effluent reveal no indication of chromatographic separation of high-Mw from low-Mw polymer species.

We appreciate how one might suspect that IAPV is tied to the tailing phenomenon. However, based on the above considerations, our observations are inconsistent with what has been attributed to IAPV.

SI Metric Conversion Factors	
$\text{c p} \times 1.0^*$	$\text{E}-03 = \text{Pax s}$
$\text{ft} \times 3.048^*$	$\text{E}-01 = \text{m}$
$\text{in.} \times 2.54^*$	$\text{E}+00 = \text{cm}$
$\text{md} \times 9.869\ 233$	$\text{E}-04 = \mu\text{m}^2$
$\text{psi} \times 6.894\ 757$	$\text{E}+00 = \text{kPa}$

*Conversion is exact.